Ocean Dynamics manuscript No.
(will be inserted by the editor)

Multiple Timescales of Stochastically Forced North Atlantic Ocean Variability: A model study

J.V. Mecking · N.S. Keenlyside · R.J. Greatbatch

Received: date / Accepted: date

J.V. Mecking
GEOMAR Helmholtz Centre for Ocean Research Kiel
Düsternbrooker Weg 20, 24105 Kiel, Germany
Present address:
Ocean and Earth Science
National Oceanography Centre Southampton
University of Southampton
SO14 3ZH, UK
Tel.: +44 2380 59 4064
E-mail: j.mecking@noc.soton.ac.uk

N.S. Keenlyside
Geophysical Institute and Bjerknes Centre, University of Bergen
Bergen, Norway

R.J. Greatbatch
GEOMAR Helmholtz Centre for Ocean Research Kiel
Düsternbrooker Weg 20, 24105 Kiel, Germany

Abstract The Atlantic meridional overturning circulation (AMOC) and the subpolar gyre (SPG) are important elements in mechanisms for multidecadal variability in models in the North Atlantic Ocean. In this study, a 2000 year long global ocean model integration forced with the atmospheric patterns associated with a white noise North Atlantic Oscillation (NAO) index, is shown to have three distinct timescales of North Atlantic Ocean variability. First, an interannual timescale with variability shorter than 15 years, that can be related to Ekman dynamics. Second, a multidecadal timescale, on the 15-65 year range, that is mainly concentrated in the SPG region and is controlled by constructive interference between density anomalies around the gyre and the changing NAO forcing. Finally, the centennial timescales, with variability longer than 65 years, that can be attributed to the ocean being in a series of quasi-equalibrium states. The relationship between the ocean's response and the NAO index differs for each timescale; the 15 year and shorter timescales are directly related to the NAO of the same year, 15-65 year timescales are dependent on the NAO index in the last 25-30 years in a sinusoidal sense while the 65 year and longer timescales relate to a sum of the last 50-80 years of the NAO index.

Keywords North Atlantic · NAO · Atlantic Multidecadal Variability · AMOC · Subpolar gyre · Stochastic · OGCM

1 Introduction

With the current increasing concern over anthroprogenic climate change, it is becoming more important to understand the natural variability in the Earth's climate system. The ocean plays an important role in the global climate system, with the North Atlantic carrying the largest part of the oceanic northward heat transport (Wunsch (2005)). The typical conveyer belt schematic of the large-scale global ocean circulation depicts both vertical and horizontal flows (Broecker et al (1991)). In the observational record of North Atlantic sea surface temperature (SST) a multidecadal signal with a period of approximately 75 years is present (Kerr (2000), Enfield et al (2001) and Knight et al (2005)), often referred to as Atlantic Multidecadal Variability (AMV) or the Atlantic Multidecadal Oscillation. This multidecadal SST signal can be seen as the fingerprint of multidecadal variability in the entire North Atlantic basin (e.g. Zhang (2008)). Unfortunately, the observational record of SST only extends back to 1870 (Rayner et al (2003)) making it difficult to determine whether or not the multidecadal signal in the SST is an internally generated oscillation or is present by chance and perhaps aided by external forcing (Otterå et al (2010), Booth et al (2012)). Of particular interest in this study are the Atlantic Meridional Overturning Circulation (AMOC) and the subpolar gyre (SPG) strength. We shall mainly be concerned with interannual to centennial variability of both the AMOC and SPG.

Within the existing proxy data (e.g. ice cores and corals) and model data (e.g. AMOC and SPG strength) various timescales of multidecadal variability have been shown ranging from 20 year timescales (e.g. in models: Dong and Sutton (2005), Born and Mignot (2012) and in proxy data: Chylek et al (2011)) to multidecadal and longer timescales (e.g. in models: Menary et al (2012) and in proxy data: Svendsen et al (2014)). It is not uncommon to find variability on multiple timescales present in the North Atlantic Ocean at the same time; again, this effect is not only seen in model data (e.g. Alvarez-Garcia et al (2008), Park and Latif (2011) and Delworth and Zeng (2012)) but also in proxy data (e.g. Saenger et al (2009) and Chylek et al (2012)). However, in order to be able to decrypt the physics behind this variability it is useful to turn to modelling studies.

Several modelling studies have looked into explaining the mechanisms behind multidecadal variability in the North Atlantic (e.g. Dijkstra et al (2006), Born and Mignot (2012) and Medhaug et al (2012)). In many cases these mechanisms involve convection in the northern regions of the North Atlantic (Delworth et al (1993), Born and Mignot (2012) and Medhaug et al (2012)). In particular, the Labrador Sea is an important region for deep convection, as seen in both modelling studies (e.g. Medhaug et al (2012)) and in observations (e.g. Dickson et al (1996)). Unfortunately, most coupled atmosphere-ocean models often have difficulty placing the convection in the correct locations, with the convection favouring the region south of Greenland and/or the Irminger Sea (Born and Mignot (2012), Ba et al (2014)) as opposed to the Labrador Sea and Greenland Sea as seen in observations (Dickson et al (1996) and de Boyer Montégut et al (2004)). An increase in convection in the northern

North Atlantic often leads to an increase in the strength of the AMOC after a few years (e.g. Delworth et al (1993), Medhaug et al (2012) and Ba et al (2014)). Several studies have shown that various North Atlantic atmospheric patterns are important in driving or exciting the multidecadal variability in the North Atlantic (e.g. Eden and Jung (2001), Medhaug et al (2012) and Langehaug et al (2012)), among these often the most important atmospheric pattern is the North Atlantic oscillation (NAO).

The NAO, the dominant atmospheric pattern in the winter North Atlantic sector (Hurrell (1995)), is a measure of the strength of the westerly winds blowing across the North Atlantic (e.g. Greatbatch (2000)). The integrated effect of the NAO on the ocean has been seen through observational data (e.g. Curry and McCartney (2001)), analytical analysis and simple models (Zhai et al (2014)). Eden and Willebrand (2001) showed that an ocean-only model forced with fluxes associated with the NAO reproduces almost all of the variability in the meridional heat transport at 48°N simulated by the same model forced with full atmospheric fluxes (correlation of 0.9). Furthermore, studies have shown that variability on multidecadal timescales in the North Atlantic can be excited by NAO forcing alone (e.g. Eden and Jung (2001)) and there is the potential for certain timescales of variability to be favoured (Visbeck et al (1998), Krahmann et al (2001) and Eden and Greatbatch (2003)).

Previous ocean-only modelling studies investigating the response to NAO forcing have considered NAO forcing of either a single sign (Eden and Willebrand (2001), Lohmann et al (2009b)), with specified frequencies (Visbeck et al

(1998), Krahmann et al (2001)) or with the historical evolution of the NAO index (Eden and Jung (2001)). These restrictions limited the previous studies to examining a relatively short timespan of model output. Mecking et al (2014) used an ocean general circulation model (OGCM) forced with a 2000 year long white noise NAO, and thus avoid these restrictions. This model setup is capable of generating multidecadal to centennial variability in the North Atlantic Ocean, with the AMOC index and the SPG strength showing different temporal characteristics in their responses to the NAO forcing, without any preferred periodicity. In this paper we continue the analysis of this 2000 year long NAO forced model integration with the goal of gaining an insight into the mechanisms behind the different timescales in the model response to the NAO forcing. Section 2 gives an overview of the model setup used in this study. Section 3, introduces the different timescales - interannual, multidecadal and centennial - seen in the AMOC at 30°N and the SPG strength. Previous studies have typically only focused on one timescale of variability. In addition to considering three different timescales, this study uses an ocean model resolution that is much higher than that of relevant previous studies (e.g. Eden and Jung (2001), Lohmann et al (2009b)). Sections 4, 5 and 6 focus in detail on each of these three timescales. Section 7 revisits the weighted NAO integration technique from Mecking et al (2014) in which weighted moving averages of the NAO index are related to indices of the AMOC and SPG strength. Finally, the results are summarised and discussed in section 8.

2 Model set-up

The Nucleus for European Modelling of the Ocean (NEMO) ocean general circulation model (OGCM) version 3.1 is used (Madec et al, 1998) in this study. The OGCM is used with the tri-polar ORCA05 grid, which has a horizontal resolution of approximately 0.5°, with slightly higher meridional resolution towards the poles, and 46 vertical levels varying from a 6 m thickness at the surface to 550m at depth (Madec and Imbard (1996)). The Drakkar parameter configuration (The Drakkar Group (2007)), which has been successfully used in previous modelling studies (see Barnier et al (2006)), is used in this study. A surface salinity restoring of 150 days to climatology is employed to avoid model drift, partial steps are used to increase bottom resolution and the Gent and McWilliams (1990) eddy parameterisation is applied. An interactive sea ice model, LIM2, is also included in this model set-up (Timmermann et al, 2005). The atmospheric forcing used in this modelling study is based on the 10 m temperature, 10 m winds, 10 m humidity, shortwave radiation, longwave radiation and precipitation from the COREv2 dataset (Large and Yeager (2004), Large and Yeager (2009)) .

The stochastically forced (SF) model experiment used in Mecking et al (2014) is analysed in this study. In this experiment, the OGCM is forced by atmospheric forcing associated with a monthly white noise NAO index, using a technique similar to that in Eden and Jung (2001) (see sections 2.2 and 2.3 from Mecking et al (2014) for a detailed explanation). The SF forced integration is started from year 725 of a climatological model integration using climatological (normal year) forcing from the COREv2 dataset (Large and Yeager (2004), Large and Yeager (2009)) and then run for 2000 years using a white noise NAO forcing (Figure S1a). The first 150 years were omitted from the analysis to avoid any shock caused by switching from climatological to interannually varying forcing.

The current model setup has been chosen since it has a global ocean configuration with a resolution higher than any previous studies of the same type, as well as, being able to sustain a stable AMOC circulation. In the previous study, Mecking et al (2014), the model setup using the observed NAO forcing was shown to be capable of simulating the multidecadal variability observed in the high latitude North Atlantic SSTs. Furthermore, this experiment is able to capture some of the more prominent features in the AMOC at 30°N and SPG strength in a model integration that uses the full atmospheric forcing fields based on reanalysis, in particular the drop in both the AMOC at 30°N and SPG strength around 1975.

All model results in this study are presented based on an annual temporal resolution. Typically an annual mean is used but in some cases the annual maximum or a mean over the winter months is used instead. Hence, in the results presented in this study the lowest period resolved is 2 years in the power spectrum and when computing cross-correlations the lead/lags all have one year spacing.

2.1 Atmospheric Forcing

In the current setup the model is forced with the 10 m temperature, winds and specific humidity, long- and shortwave radiation and precipitation as opposed to the fluxes directly. Therefore the heat, momentum and fresh water fluxes are computed by the ocean model and can vary with the state of the ocean. The resulting heat flux forcing associated with the NAO does not differ much from what is expected from observations (Visbeck et al (2003), Figure 1a). As expected, the positive minus negative NAO difference is associated with a large area of upward heat flux over the Labrador Sea and a narrow region from the east coast of Greenland up to Svalbard. The winter vertical component of wind stress curl (hereafter just referred to as wind stress curl) associated with the positive minus negative NAO difference shows a mostly positive curl north of approximately 55°N, with the main exceptions being along the eastern coasts of Canada and Greenland. South of 55°N, the wind stress curl is mostly negative (Figure 1b). It should be noted that the surface fluxes are computed using the bulk formulae from the input atmospheric fields and the ocean model output (in particular the ocean SST and the ocean surface velocity, the latter being used in the computation of the surface wind stress). Since the bulk formulae are nonlinear, there is no guarantee that the fluxes that force the model have the same white spectrum as the input atmospheric variables. For wind stress curl over the SPG region, there is not much difference in the power spectrum from that of the white noise used for the NAO index (Figure S1a,c). However, the power spectrum for the surface heat flux over the SPG region shows a distinct reddening (Figure S1b). Surface heat flux is proportional to the difference between the surface air temperature and SST. While SST variations themselves result from fluctuations in surface heat flux and oceanic processes, which lead to a reddening of the SST and thus a reddening of the heat flux spectrum.

3 Model results

Ocean convection, an important component in several mechanisms of the AMOC (Dickson et al (1996)), is measured by means of the surface mixed layer depth, here defined as the depth at which the potential density (referenced to the surface) differs from the surface value by 0.1 kg/m^3. The mixed layer depth, using this definition, is given as standard model output from NEMO and we believe it gives good insight towards the convective behaviour of the model. In our simulations the main convection regions in the North Atlantic region are the Labrador and Greenland Seas (Figure 2a). The Greenland Sea convection region is found right at the ice edge (Figure 2a) and with the exception of approximately 5 years, the maximum mixed layer depth in each year throughout the 2000 year long SF model integration is always greater then 3000 m (not shown). This in contrary to the sea saw hypothesis put forth by Dickson et al (1996), where convection in the Labrador Sea is in phase with the NAO and the convection in the Greenland Sea is out of phase with the NAO, since here there is no variability in the Greenland Sea convection.

Both the AMOC and SPG form important parts of the ocean circulation in the North Atlantic Ocean basin. The Atlantic meridional streamfunction is defined as follows:

$$AMOC(y,z,t) = \int_{west}^{east} \int_{-H}^{z} v(x,y,z',t)dz'dx, \quad (1)$$

where $v(x,y,z,t)$ is the meridional velocity in the Atlantic Basin minus the Atlantic section mean meridional velocity at each latitude (to remove the barotropic transport component) and $H = H(x,y)$ is the ocean depth. The mean AMOC streamfunction from the SF integration shows both the positive North Atlantic Deep Water circulation cell and the negative Antarctic Bottom Water circulation cell (Figure 2b - Figure 4b from Mecking et al (2014)). The maximum in the AMOC streamfunction occurs near 30°N and at a depth of 793 m with a value of 13.25 Sv. The maximum value of the AMOC is weaker than in observations (18.7 Sv according to Cunningham et al (2007)) but still falls within the range of ocean-only models (Griffies et al, 2009). Therefore we choose to define the AMOC index in this study as the maximum value of the meridional streamfunction at 30°N (Figure 2b,3b). Some properties of the AMOC at 30°N were already discussed in Mecking et al (2014); in this study they will be examined more closely. Of particular interest is the abrupt change in the power spectrum at a period of about 65 years (Figure 4a); in this case a first order autoregressive (AR(1)) process is clearly not a good fit for the AMOC spectrum at 30°N (Mecking et al, 2014).

The mean barotropic streamfunction from the SF integration in the North Atlantic models shows both the counterclockwise SPG and the clockwise subtropical gyre (Figure 2c). The SPG strength is defined as the mean of the annual mean barotropic streamfunction averaged over the region 60°W to 15°W, 48°N to 65°N as in Lohmann et al (2009a) (Figure 2c; Figure 4c from Mecking et al (2014)), which is then multiplied by -1 allowing positive values the SPG strength to indicate an increase in gyre strength. As with the AMOC at 30°N, although the SPG strength shows stronger variability at low frequencies than at high frequencies, an AR(1) process is not an ideal fit (Mecking et al, 2014). However, the transition to the long timescales of variability is not as abrupt as for the AMOC at 30°N (Figure 4b). The power spectrum of the SPG strength shows much stronger variability in the middle range timescales (15-65 years) than the power spectrum of the AMOC at 30°N. However, the power spectrum of the SPG strength shows a sharp drop in spectral power at approximately 65 years (Figure 4b). This suggests dividing the time series into 3 different frequency bands; the interannual (timescales shorter than 15 years; changing the cut-off by ±5 years does not alter the results significantly), the multidecadal (timescales of 15-65 years) and the centennial (timescales longer than 65 years). The timeseries were then filtered using a fifth order Butterworth filter in order to separate the interannual, multidecadal and centennial timescales; that is using a high pass filter with 15 year cut off, a band pass filter with a 15-65 year band and a low pass filter with a 65 year cut off, respectively (Figures 3, 4; red, green and blue colouring). The amplitude of the variability in the AMOC at 30°N is clearly weaker on the 15-65 year timescale relative to the 65 year and longer timescale, while the amplitude variability of the SPG strength does not differ much between the 15-65 year timescale and the 65 year and longer timescale (Figure 3). Similar to the AMOC at 30°N, the mixed layer depth in the Labrador Sea also has a weaker variability on the 15-65 year timescale than on the 65 year and longer timescale (Figure 3).

The following sections focus on describing the properties of the interannual (15 years and shorter), the multidecadal (15-65 years) and centennial (65 years and longer) timescales in more detail.

4 Interannual Timescale

Computing the cross-correlations between the 15 year high pass filtered NAO, AMOC at 30°N, and SPG strength shows that there are strong correlations in phase with the NAO index and the correlation quickly drops off thereafter (Figure 5a,b). The AMOC at 30°N is positively correlated with the NAO with a significant correlation of 0.70 at 0 lag (Figure 5a). On lags of one year and longer, the correlation between the the NAO index and the AMOC at 30°N changes sign and becomes very small but remains significant (Figure 5a). The SPG strength and the NAO index have a significant negative correlation of -0.74 at 0 lag, and the correlation again becomes very small and changes sign at larger lags (Figure 5b). This result is similar to Eden and Willebrand (2001) where the initial response of the SPG to the NAO changes sign after about 3 years.

The barotropic streamfunction associated with a positive NAO minus negative NAO index has a large area of positive barotropic streamfunction (spin-down of the SPG) covering much of the North Atlantic (Figure 6a) and a weaker negative anomaly over the region surrounding Iceland. Comparing the anomalies in the barotropic streamfunction to the mean SPG (Figure 2c and Figure 6a) shows that the associated spin-down of the SPG on the interannual timescales corresponds to a decrease in the western part of the gyre only. The circulation in the Nordic Seas is in contrast enhanced. The response of the barotropic streamfunction to the wind forcing is what is expected from the topographic Sverdrup relationship (Figure 6a and Figure 1b[1]) as noted by Eden and Willebrand (2001).

The AMOC pattern associated with the 15 year high pass filtered positive NAO minus negative NAO index shows two cells of meridional overturning; one with a positive overturning centred at 30°N with a maximum at a depth of about 2.5 km and the other with a negative overturning centred at about 50°N and with maximum at a depth of about 0.5 km (Figure 6b). This overturning cell, with Ekman transport in the surface layer, is what is expected from the directly wind driven AMOC. Previous studies have shown that interannual variability in the AMOC is strongly related to the atmospheric forcing (Roberts et al (2013)), in particular the interannual AMOC variability can be linked to the NAO (Atkinson et al (2010)). Therefore to help explain the

[1] Note that using the high pass filtered NAO index as opposed to the unfiltered NAO index to compute the wind stress curl pattern gives an almost identical result.

double cell structure in the AMOC, we again turn to the wind stress curl. Since the 15 year high pass filtered AMOC at 30°N is positively correlated with the NAO (Figure 5a) we can compare with the wind stress curl pattern in Figure 1b. From Ekman pumping, $\rho w = f\hat{k} \cdot (\nabla \times \bar{\tau})$, where ρ is the density, w is the vertical velocity at the bottom of the Ekman layer and τ is the wind stress, we know that a positive (negative) wind stress curl will lead to upward (downward) Ekman pumping. From Figure 1b, the positive wind stress curl centred near 65°N coincides with a region of anomalous upwelling at 65°N and the negative wind stress curl centred at 45°N coincides with the region between the two cells where there is anomalous sinking (Figure 6b).

For the interannual timescales it is clear that the SPG strength and the AMOC variability is strongly associated with the immediate response of the ocean to the wind stress through the Ekman dynamics, similar to the results from Eden and Willebrand (2001).

5 Multidecadal Timescale

From the power spectrum (Figure 4a,b) and the filtered timeseries (Figure 3, green) it is evident that the AMOC at 30°N does not have a very strong signal on the 15-65 year timescale; in contrast the SPG strength and AMOC at higher latitudes has a more prominent signal on these time scales. The standard deviation of the AMOC when filtered with a 15-65 year band pass filter shows that the area of strongest variability, with a standard deviation of 0.4 Sv, is centred at approximately 48°N and a depth of 2 km (Figure

S2a). Figure S2b shows that the power spectrum of the time series of the maximum AMOC at 48°N more closely resembles the power spectrum of the SPG strength (Figure 4b) than does the power spectrum of the AMOC at 30°N (Figure 4a). The power spectrum of the SPG strength has a local maximum at 33 years in the multidecadal timescales range (Figure 4b). However, this peak in the power spectrum is relatively broad suggesting oscillatory periods can range around this period.

The auto-correlation of the filtered AMOC at 30°N and SPG strength timeseries show minima at ±13 years lag, suggesting an oscillation with a period of approximately 26 years (Figure 5c,d). The cross-correlation between the filtered AMOC at 30°N and NAO indices shows a significant correlation with a maximum of 0.34 when the NAO leads by 8 years (Figure 5c). The cross-correlation of the filtered SPG strength and NAO indices has a maximum significant correlation of 0.69 with the NAO leading by 6 years (Figure 5d). Despite the AMOC at 30°N having a weak signal on multidecadal timescales it lags the SPG strength by 4 years with a significant correlation of 0.66, similar to the relationship between the SPG strength and AMOC seen in Lohmann et al (2009b).

The spatial pattern of the barotropic streamfunction associated with the years in which the SPG strength is a maximum minus the years in which the SPG strength is a minimum shows a negative anomaly of the barotropic streamfunction covering a similar region as the mean SPG (Figure 2c,7c). The pattern in the barotropic streamfunction 14 years before maximum in

SPG strength is similar to Figure 7c but with the opposite sign (not shown); the same is true when using data from 14 years after the extrema in SPG strength. This indicates an oscillatory behaviour with a period of approximately 28 years. Density in the centre of the gyre is an important aspect of mechanisms for SPG strength variability; in the study of Born and Mignot (2012), a maximum in density at the centre of the SPG occurs in phase with the maximum in SPG strength. The density of the upper 208 m (upper 14 model levels and approximate mean mixed layer depth in that region) shows a maximum density in the centre of the gyre region 7 years before the maximum in SPG strength occurs (Figure 7b). The maximum surface density anomaly over the SPG occurs in phase with a positive NAO index and leads to a pattern in the barotropic streamfunction similar to the pattern in phase with the 15 year high pass filtered NAO (Figure 6a,7a). A density anomaly of the opposite sign appears 7 years after the maximum in SPG strength (not shown) leading to an oscillatory cycle of approximately 28 years.

To further investigate the density signal in the centre of the gyre an annual mean potential density profile is made in box C in Figure 8. Lagged composite analysis of the potential density profile and the 15-65 year band pass filtered SPG strength shows that the density anomaly reaches its maximum depth almost in phase with the 15-65 year filtered SPG strength (Figure S3). However, as before, a maximum in surface density anomaly is found 7 years before a maximum in SPG strength and appears to be confined to the mixed layer (Figure 9a).

When examining year by year the density anomalies associated with the 15-65 year band pass filtered SPG strength, density anomalies appear to be propagating around the SPG. In the studies of Sutton and Allen (1997) and Alvarez-Garcia et al (2008), SST anomalies propagate along the Gulf Stream and then along the North Atlantic Current on multidecadal timescales. This propagation of SST anomalies is too slow to be associated with the mean currents, suggesting it has to either be related to currents below the surface, currents not in the strongest part of the Gulf Stream, anomalous advection or some other mechanism (Sutton and Allen (1997)). Here we have setup profiles along the path of the SPG (Figure 8, red boxes). Tracing the density anomalies around the SPG using the 15-65 year band pass filtered SPG strength shows that anomalies propagate around the SPG with a period of approximately 25 years (Figure 9a). Density anomalies from box 1 make their way relatively slowly to box 4-6 taking approximately 15 years. This density anomaly takes another 10 years to go from box 6 back to box 1 to complete the cycle (Figure 9a). These timescales are similar to what is found in the studies of Sutton and Allen (1997) and Alvarez-Garcia et al (2008).

The ≈26-28 year periodicity in the SPG can be understood in terms of a positive interference between the advection of density anomalies around the gyre and the NAO-related wind forcing. First, note in contrast to the heat fluxes, wind stress curl spectra is essentially white and does not exhibit a minimum on multidecadal timescales (Figure S1); furthermore the pattern of the wind stress curl associated with the NAO on these timescales is almost identical to Figure 1b with a smaller amplitude, as expected. Consider NAO variations with ≈26 year periodicity. During the positive NAO phase wind stress curl is negative over the region containing boxes 8 and 1 (Figure 9b), leading to downwelling, and in turn an increase in temperature in the upper layers, due to warm surface waters being brought down to deeper depths, and a decrease in density (Figure 9a). This decrease in density originates along the Labrador Current where the wind stress curl due to the NAO is strongest (Figures 1b,7b). After 10-15 years this anomaly will propagate to boxes 4, 5, and 6. The NAO is now negative, and wind stress curl over boxes 4,5, and 6 is negative (Figure 9b), which reinforces the anomalies advected from boxes 8 and 1. After another ≈10 years, the anomalies will have propagated back to boxes 8 and 1, the NAO will again be positive, and the anomalies will be further reinforced (Figures 9a,b). Thus, there is a constructive interference when NAO periodicity matches the advective timescale of the SPG. This argument holds equally when starting with a negative NAO, but in the opposite sense. Performing similar analysis with the heat fluxes (not shown) does not show very strong connections on these timescales and for some points along the path the heat flux creates destructive interference. The mechanism described above is reminiscent of that described by Krahmann et al (2001), and analogous to the mechanism proposed by Saravanan and McWilliams (1998). In our model simulation the preferred timescale for variability is slightly longer than the timescale with the strongest response in the ocean in Krahmann et al (2001). However, in Sutton and Allen (1997) it takes the temperature anomalies ≈6 years to propagate along the North Atlantic Current part of the gyre (from the 3500 km to the 7000 km points in Figure 2a of Sutton and Allen (1997)), similar to the propagation time presented here (≈6 years from box 2-4, Figure 9a).

In summary, the multidecadal (15-65 year) timescale shows strong variability in the SPG region. A density anomaly located in the upper 208 m at the center of the SPG leads the SPG strength by 5-7 years and when this anomaly reaches its maximum depth it becomes in phase with the SPG strength. The variability of the multidecadal timescale is related to the propagation of density anomalies around the SPG and their constructive interference with density anomalies generated by the wind stress related to the NAO on these timescales.

6 Centennial Timescale

The power spectra of both the AMOC at 30°N and the SPG strength show strong variability on the 65 year and longer timescales (Figure 4a,b, blue). The flattening out of the spectrum on these timescales is an indication that the model has a quasi-equalibrium response to the applied forcing. Furthermore, from the work done in Mecking et al (2014), we know that the signals on the long timescales are a response to the low frequency signal in the white noise NAO index.

The cross-correlation analysis of the 65 year low pass filtered data has the NAO leading the AMOC at 30°N (SPG strength) by 36 (15) years with a significant correlation of 0.68 (0.61) (Figure 5e,f). Furthermore, the auto- and cross-correlation analysis of the 65 year low pass filtered timeseries shows no indication of a possible oscillatory behaviour; for all auto- and cross-correlation curves the largest correlation is positive and significant at 95% but none of the negative correlations are significant (Figure 5e,f). The lack of a significant negative correlation in the auto-correlation suggests that there is no oscillation present on these timescales. In the 65 year low pass filtered timescales, the mixed layer depth in the Labrador Sea has a strong signal (Figure 3); this signal is in phase with the AMOC at 30°N with a correlation of 0.94. The mixed layer depth in the Labrador Sea plays an important role on the centennial timescales with the Labrador Sea being the main region of convection on these timescales (not shown). Similar to the coupled model study by Ba et al (2013) on multidecadal (periods $>$ 50 years) to centennial timescales the salinity dominates the mixed layer density variability and the temperature only plays a minor damping role (Figure S5). This also supports the results by Huang et al (2014), where they show that in the majority of coupled models they examined, salinity dominates the convection on long timescales.

The spatial pattern of the AMOC associated with the quasi-equalibrium states on the centennial timescales is essentially single signed with a maximum centred at about 35°N and at a depth of 1.5 km (Figure 10a). The pattern of a persistent positive minus negative AMOC suggests that the upper overturning cell strengthens and deepens (weakens and shallows) during a persistent phase of positive (negative) AMOC at 30°N, while the lower, weaker overturning cell is only very marginally weakened (strengthened) (Figures 10a,2b). The barotropic streamfunction associated with the maximum minus minimum in SPG strength on the 65 year and longer timescales shows that the SPG spins-up with persistent positive NAO forcing and spins-down with persistent negative NAO forcing (Figure 10b,5f).

On the centennial (65 year and longer) timescales both the power spectra and auto-correlation analysis indicates that the ocean model is in a series of quasi-equalibrium states requiring several years to set-up. More evidence for the series of quasi-equalibrium states comes from the wavelet spectra (Figure 3 in Mecking et al (2014)) where on long periods the wavelet spectrum of the NAO is reflected in the wavelet spectrum of the AMOC.

7 NAO Integration

Examining the coefficients in a weighted NAO index reconstruction of the AMOC index and SPG strength helps shed further light on the different relationships between the NAO forcing and the ocean circulation.

In Mecking et al (2014), it was shown that the AMOC at 30°N and the SPG strength in an idealised NAO forced simulation can be reconstructed by integrating the NAO index as follows:

$$index(t) = \alpha_0 + \sum_{k=1}^{q} \alpha_k NAO(t-k+1) + \xi(t), \tag{2}$$

where q is the number of years of the NAO used to compute the index (either AMOC or SPG strength), with the α_k's computed using a linear regression method and $\xi(t)$ representing a residual term. These results showed that the

AMOC can be reconstructed using 53 previous years of the NAO with a correlation of 0.67 on decadal timescales (running mean of 11 years) and the SPG strength can be reconstructed using 10 previous years of data with a correlation of 0.61 on decadal timescales. However, the reconstruction of the SPG strength can be improved by extending the number of years of the NAO used to at least 50 years. Upon closer examination we see that the reconstruction using only 10 years of the NAO index only captured the shorter timescales, and had weaker variability on the centennial timescales (Figure S4). Taking a closer look at the NAO integration coefficients reveals three distinct behaviours (Figure 11, black circles): 1) For both the AMOC and SPG strength the coefficient for the NAO at lag 0 (i.e. α_1) is very large and in the case of the SPG strength of opposite sign to the majority of the remainder of the coefficients. 2) In the case of the SPG strength the first 12 coefficients are large relative to the remainder of the coefficients but this distinction is not as clear in the coefficients from the AMOC at 30°N. 3) The coefficients up to approximately 75 years for the AMOC and 50 years for the SPG strength are all relatively small and positive.

Using the filtered timeseries to compute the integrated NAO[2] fits, reveals the different behaviours on the different timescales (Figure 11a,b). On the interannual timescales both the AMOC at 30°N and the SPG strength have large values for the first few coefficients, with α_1 being the largest by far and of

[2] For the integrated NAO fits, the time series being reconstructed were filtered but the NAO index used remained unfiltered.

opposite sign for the AMOC and the SPG strength (Figure 11, red triangles). The opposite sign of the first and second coefficient supports the change of sign in the response to the NAO in the AMOC index and SPG strength after 2-3 years from the initial response. For the long time scales the behaviour of the integrated NAO coefficients are similar for both the AMOC index and the SPG strength, all having relatively small, positive values for 75 and 50 years, respectively, (Figure 11, blue triangles). This implies that having persistent NAO forcing for at least 50 years will be reflected in the AMOC and SPG strength timeseries, adding to the evidence that on the centennial timescales the ocean is in a quasi-equilibrium state requiring about 50 years to setup. The coefficients for the multidecadal timescale reconstruction are almost zero in the case of the AMOC index (Figure 11a, green triangles), supporting the evidence that there is only very weak variability on these timescales. However, for the SPG strength, the integrated NAO coefficients for the 15-65 year timescales show an interesting behaviour, with the coefficients having a sinusoidal shape with a maximum at approximately α_8 and minimum at approximately α_{17} giving a period of roughly 8+17=25 years (Figure 11b, green triangles). The sinusoidal shape of the α's has the consequence of enhancing the power at timescales with similar period, causing the broad peak at near 25 years in the power spectrum of the SPG strength and reducing the amplitude of variability on longer timescales leading to the drop in the amplitude of the variability at time scales near 60 years (Figure 4b). Summing the integrated NAO coefficients computed from the filtered timeseries gives the NAO coefficients from the unfiltered timeseries. In particular, in the SPG strength case, summing the integrated NAO coefficients from the 65 year low pass filtered timescales with the 15-65 year band pass filtered integrated NAO coefficients from α_{15} to α_{25} leads to these coefficients becoming zero. This lead to the initial hypothesis that reconstructing the SPG strength only required 10 years of NAO data (Mecking et al (2014)), however, it underestimated the centennial timescales Figure S4).

8 Conclusions and Discussion

This paper continued the analysis of the 2000 year long stochastically forced (SF) model integration introduced in Mecking et al (2014), describing the various timescales of variability. Through analysis of the power spectra of the AMOC at 30°N and the SPG strength, the model output was divided into three different timescales of variability: interannual (15 years and shorter), multidecadal (15-65 years) and centennial (65 years and longer). A short summary of the model behaviour follows:

– On the interannual timescales the first coefficient of the integrated NAO fit is the largest, suggesting a strong immediate response to the NAO. The response to the NAO forcing on these timescales is mainly driven by Ekman dynamics as in Eden and Willebrand (2001), with the delayed response most likely wind driven. The SPG spins down for positive values of the NAO due to the topographic Sverdrup response to the wind forcing. The AMOC generates two anomalous overturning cells, a positive one centred at 30°N and a negative one centred at 50°N; these are mainly due to the effects of downward Ekman pumping and Ekman upwelling associated with the wind stress curl.

- The multidecadal (15-65 year) timescales have integrated NAO coefficients for the SPG strength that have the shape of approximately one period of a sinusoid. This multidecadal timescale is dominated by variability in the SPG with a period of around 26-28 years and can be related to density changes in and around the centre of the gyre. The reinforcement of variability on these timescales is due to the constructive interference of the density anomalies being advected around the SPG and the NAO generated wind stress curl forcing on these timescales, similar to the mechanism discussed in Krahmann et al (2001).

- The centennial timescale has integrated NAO coefficients that are all positive and have nearly the same value. These integrated NAO coefficients are non-zero for the first 75 years in the reconstruction of the AMOC at 30°N and for the first 50 years of the SPG strength. Evidence from the centennial timescales suggests that the ocean model variability is in a series of quasi-equilibrium states in response to the changing forcing on these timescales.

This study examines the behaviour of an ocean-only model to a stochastic NAO forcing, focusing on variability present on 3 different timescales. For two of the timescales the variability resembles what has been seen in previous ocean-only modelling studies investigating the response to the NAO: the behaviour at interannual timescales resembles what was found in the study by Eden and Willebrand (2001), and the multidecadal variability resembles the results from Lohmann et al (2009b) and Krahmann et al (2001). The response to centennial and longer timescale NAO forcing has previously not been investigated in an ocean-only context. We do not find much evidence for a non-linear response to NAO forcing, since it is possible to reconstruct the AMOC at 30°N and SPG strength using a linear combination of the NAO forcing for different years.

It is well known that the anomalous patterns associated with positive and negative NAO are not just inverses of each other with the positive NAO having the centers of the high and low pressure regions shifted eastward relative to a negative NAO (Peterson et al (2003)). Indeed, the forcing patterns used in Lohmann et al (2009b) for their positive and negative NAO experiments differ from each other, since they base their forcing patterns on composites when the NAO is positive, neutral or negative separately. In the present study we restrict ourselves to the pattern resulting from regressing atmospheric variables on the NAO index resulting in positive and negative anomalies in surface fluxes that are roughly the negative of each other. Consistently, we do not find substantial differences in composites based only on positive or only on negative NAO anomalies (not shown). We do not expect that accounting for differences in

NAO positive and negative patterns would substantially change any of our conclusions on simulated variability.

Coupled modelling studies have simulated variability on a wide range of timescales, with little consensus on preferred periodicity and atmospheric forcing pattern (e.g. Medhaug et al (2012), Wang and Zhang (2013), Ba et al (2014)). For the most cases the coupled models examined in the discussion section of Mecking et al (2014), show that the AMOC at 30°N has weaker variability on timescales around 20 years than an AR(1) process. However, in the coupled models this effect is not as clear as in the ocean-only model forced with only the NAO analysed here. This indicates that other processes could be enhancing the multidecadal variability in the lower latitudes in these models, whether it be from atmospheric modes of variability other than the NAO or atmosphere/ocean interactions not present in the ocean-only setup used in the present study. Nevertheless, we hope that our results from this study can be useful in helping interpret results from coupled climate models.

Using the method of integrating the NAO to investigate ocean model experiments can be a useful technique to gain insight into the dynamics on different timescales. This method could be applied to the results from coupled atmosphere-ocean models and can be extended to include other atmospheric forcing patterns. For example, the Scandinavian pattern (Barnston and Livezey, 1987) could be included allowing for possible effects related to convection in the Greenland Sea and the Greenland-Scotland overflows (Medhaug et al, 2012). This relatively simple method can be useful, without being computationally expensive, in making predictions (similar to Eden et al (2002)), as well as in inter-model comparisons.

Acknowledgements The comments from two anonymous reviewers were very much appreciated and helped improve the manuscript. We would also like to thank Florian Sévellec for some useful discussions. We would like to acknowledge the support from the DFG Emmy Noether-Programm (Grant KE 1471/2-1), GEOMAR and the HLRN computing facility. NK acknowledges support from the NFR EPOCASA (Grant 229774/E10), EU-STEPS (PCIG10-GA-2011-304243) and EU-PREFACE (GA 603521) projects.

References

Alvarez-Garcia F, Latif M, Biastoch A (2008) On multidecadal and quasi-decadal north atlantic variability. Journal of Climate 21(14):3433–3452, DOI 10.1175/2007JCLI1800.1

Atkinson C, Bryden H, Hirschi J, Kanzow T (2010) On the seasonal cycles and variability of florida straits, ekman and sverdrup transports at 26 n in the atlantic ocean. Ocean Science 6(4):837–859, DOI 10.5194/os-6-837-2010

Ba J, Keenlyside NS, Park W, Latif M, Hawkins E, Ding H (2013) A mechanism for Atlantic multidecadal variability in the Kiel Climate Model. Climate Dynamics pp 1–12, DOI 10.1007/s00382-012-1633-4

Ba J, Keenlyside NS, Latif M, Park W, Ding H, Lohmann K, Mignot J, Menary M, Otterå OH, Wouters B, et al (2014) A multi-model comparison of atlantic multidecadal variability. Climate Dynamics pp 1–16, DOI 10.1007/s00382-014-2056-1

Barnier B, Madec G, Penduff T, Molines J, Treguier A, Le Sommer J, Beckmann A, Biastoch A, Böning C, Dengg J, et al (2006) Impact of partial steps and momentum advection schemes in a global ocean circulation model at eddy-permitting resolution. Ocean Dynamics 56(5):543–567, DOI 10.1007/s10236-006-0082-1

Barnston A, Livezey R (1987) Classification, seasonality and persistence of low-frequency atmospheric circulation patterns. Monthly Weather Review 115(6):1083–1126

Booth BB, Dunstone NJ, Halloran PR, Andrews T, Bellouin N (2012) Aerosols implicated as a prime driver of twentieth-century north atlantic climate variability. Nature 484(7393):228–232, DOI 10.1038/nature10946

Born A, Mignot J (2012) Dynamics of decadal variability in the atlantic subpolar gyre: a stochastically forced oscillator. Climate dynamics 39(1):461–474, DOI 10.1007/s00382-011-1180-4

de Boyer Montégut C, Madec G, Fischer AS, Lazar A, Iudicone D (2004) Mixed layer depth over the global ocean: An examination of profile data and a profile-based climatology. Journal of Geophysical Research: Oceans (1978–2012) 109(C12), DOI 10.1029/2004JC002378

Broecker WS, et al (1991) The great ocean conveyor. Oceanography 4(2):79–89

Chylek P, Folland C, Dijkstra H, Lesins G, Dubey M (2011) Ice-core data evidence for a prominent near 20 year time-scale of the Atlantic Multidecadal Oscillation. Geophysical Research Letters 38(13):L13,704, DOI 10.1029/2011GL047501

Chylek P, Folland C, Frankcombe L, Dijkstra H, Lesins G, Dubey M (2012) Greenland ice core evidence for spatial and temporal variability of the atlantic multidecadal oscillation. Geophysical Research Letters 39(9), DOI 10.1029/2012GL051241

Cunningham SA, Kanzow T, Rayner D, Baringer MO, Johns WE, Marotzke J Longworth HR, Grant EM, Hirschi JJM, Beal LM, et al (2007) Temporal variability of the Atlantic meridional overturning circulation at 26.5 N. Science 317(5840):935–938 DOI 10.1126/science.1141304

Curry R, McCartney M (2001) Ocean gyre circulation changes associated with the North Atlantic Oscillation. Journal of Physical Oceanography 31(12):3374–3400

Delworth T, Zeng F (2012) Multicentennial variability of the Atlantic meridional overturning circulation and its climatic influence in a 4000 year simulation of the GFDL CM2. 1 climate model. Geophysical Research Letters 39(13):L13,702, DOI 10.1029/2012GL052107

Delworth T, Manabe S, Stouffer R (1993) Interdecadal variations of the thermohaline circulation in a coupled ocean-atmosphere model. Journal of Climate 6(11):1993–2011

Dickson R, Lazier J, Meincke J, Rhines P, Swift J (1996) Long-term coordinated changes in the convective activity of the North Atlantic. Progress in Oceanography 38(3):241–295

Dijkstra H, Te Raa L, Schmeits M, Gerrits J (2006) On the physics of the Atlantic Multidecadal Oscillation. Ocean Dynamics 56(1):36–50, DOI

10.1007/s10236-005-0043-0

Dong B, Sutton RT (2005) Mechanism of interdecadal thermohaline circulation variability in a coupled ocean-atmosphere gcm. Journal of climate 18(8):1117–1135, DOI 10.1175/JCLI3328.1

Eden C, Greatbatch RJ (2003) A damped decadal oscillation in the north atlantic climate system. Journal of climate 16(24):4043–4060, DOI 10.1175/1520-0442(2003)016<4043:ADDOIT>2.0.CO;2

Eden C, Jung T (2001) North atlantic interdecadal variability: oceanic response to the North Atlantic Oscillation (1865-1997). Journal of Climate 14(5):676–691, DOI 10.1175/1520-0442(2001)014<0676:NAIVOR>2.0.CO;2

Eden C, Willebrand J (2001) Mechanism of interannual to decadal variability of the North Atlantic circulation. Journal of Climate 14(10):2266–2280, DOI 10.1175/1520-0442(2001)014<2266:MOITDV>2.0.CO;2

Eden C, Greatbatch R, Lu J (2002) Prospects for decadal prediction of the North Atlantic Oscillation (NAO). Geophysical research letters 29(10):1466, DOI 10.1029/2001GL014069

Enfield D, Mestas-Nunez A, Trimble P, et al (2001) The atlantic multidecadal oscillation and its relation to rainfall and river flows in the continental U. S. Geophysical Research Letters 28(10):2077–2080, DOI 10.1029/2000GL012745

Gent P, McWilliams J (1990) Isopycnal mixing in ocean circulation models. Journal of Physical Oceanography 20(1):150–155, DOI

10.1029/2004GL019932

Greatbatch R (2000) The North Atlantic Oscillation. Stochastic Environmental Research and Risk Assessment 14(4):213–242, DOI 10.1007/s004770000047

Griffies SM, Biastoch A, Böning C, Bryan F, Danabasoglu G, Chassignet EP, England MH, Gerdes R, Haak H, Hallberg RW et al (2009) Coordinated ocean-ice reference experiments (COREs). Ocean Modelling, 26(1):1–46, DOI 10.1016/j.ocemod.2008.08.007

Huang W, Wang B, Li L, Dong L, Lin P, Yu Y, Zhou T, Liu L, Xu S, Xia K, et al (2014) Variability of Atlantic meridional overturning circulation in FGOALS-g2. Advances in Atmospheric Sciences 31(1):95–109, DOI 10.1007/s00376-013-2155-7

Hurrell J (1995) Decadal trends in the north atlantic oscillation: regional temperatures and precipitation. Science 269(5224):676–678, DOI 10.1126/science.269.5224.676

Kerr R (2000) A north atlantic climate pacemaker for the centuries. Science 288(5473):1984–1985, DOI 10.1126/science.288.5473.1984

Knight J, Allan R, Folland C, Vellinga M, Mann M (2005) A signature of persistent natural thermohaline circulation cycles in observed climate. Geophysical Research Letters 32(20):2–5, DOI 10.1029/2005GL024233

Krahmann G, Visbeck M, Reverdin G (2001) Formation and Propagation of Temperature Anomalies along the North Atlantic Current*. Journal of physical oceanography 31(5):1287–1303, DOI 10.1175/1520-

0485(2001)031i<1287:FAPOTA>2.0.CO;2

Langehaug H, Medhaug I, Eldevik T, Otterå O (2012) Arctic/Atlantic exchanges via the subpolar gyre. Journal of Climate 25(7):2421–2439, DOI 10.1175/JCLI-D-11-00085.1

Large W, Yeager S (2004) Diurnal to decadal global forcing for ocean and sea-ice models: the data sets and flux climatologies. National Center for Atmospheric Research

Large W, Yeager S (2009) The global climatology of an interannually varying air–sea flux data set. Climate Dynamics 33(2):341–364, DOI 10.1007/s00382-008-0441-3

Lohmann K, Drange H, Bentsen M (2009a) A possible mechanism for the strong weakening of the North Atlantic subpolar gyre in the mid-1990s. Geophysical Research Letters 36(15):L15,602, DOI 10.1029/2009GL039166

Lohmann K, Drange H, Bentsen M (2009b) Response of the north atlantic subpolar gyre to persistent north atlantic oscillation like forcing. Climate dynamics 32(2-3):273–285, DOI 10.1007/s00382-008-0467-6

Madec G, Imbard M (1996) A global ocean mesh to overcome the north pole singularity. Climate Dynamics 12(6):381–388, DOI 10.1007/BF00211684

Madec G, Delecluse P, Imbard M, Lévy C, et al (1998) Opa 8.1 ocean general circulation model reference manual. Note du Pôle de modélisation, Institut Pierre-Simon Laplace 11

Mecking J, Keenlyside N, Greatbatch R (2014) Stochastically-forced multidecadal variability in the North Atlantic: a model study. Climate Dynamics pp 1–18, DOI 10.1007/s00382-013-1930-6

Medhaug I, Langehaug H, Eldevik T, Furevik T, Bentsen M (2012) Mechanisms for decadal scale variability in a simulated Atlantic meridional overturning circulation. Climate dynamics 39(1–2):77–93, DOI 10.1007/s00382-011-1124-z

Menary M, Park W, Lohmann K, Vellinga M, Palmer M, Latif M, Jungclaus J (2012) A multimodel comparison of centennial Atlantic meridional overturning circulation variability. Climate dynamics 38(11):2377–2388, DOI 10.1007/s00382-011-1172-4

Otterå OH, Bentsen M, Drange H, Suo L (2010) External forcing as a metronome for Atlantic multidecadal variability. Nature Geoscience 3(10):688–694, DOI 10.1038/ngeo955

Park W, Latif M (2011) Atlantic meridional overturning circulation response to idealized external forcing. Climate Dynamics 39(7–8):1709–1726, DOI 10.1007/s00382-011-1212-0

Peterson KA, Lu J, Greatbatch RJ (2003) Evidence of nonlinear dynamics in the eastward shift of the nao. Geophysical research letters 30(2), DOI 10.1029/2002GL015585

Rayner N, Parker D, Horton E, Folland C, Alexander L, Rowell D, Kent E, Kaplan A (2003) Global analyses of sea surface temperature, sea ice, and night marine air temperature since the late nineteenth century. Journal of Geophysical Research 108(D14):4407, DOI 10.1029/2002JD002670

Roberts C, Waters J, Peterson K, Palmer M, McCarthy G, Frajka-Williams E, Haines K, Lea D, Martin M, Storkey D, et al (2013) Atmosphere drives recent interannual variability of the atlantic meridional overturning circulation at 26.5? n. Geophysical Research Letters 40(19):5164–5170, DOI 10.1002/grl.50930

Saenger C, Cohen AL, Oppo DW, Halley RB, Carilli JE (2009) Surface-temperature trends and variability in the low-latitude North Atlantic since 1552. Nature Geoscience 2(7):492–495, DOI 10.1038/ngeo552

Saravanan R, McWilliams JC (1998) Advective ocean-atmosphere interaction: An analytical stochastic model with implications for decadal variability. Journal of Climate 11(2):165–188, DOI 10.1175/1520-0442(1998)011<0165:AOAIAA>2.0.CO;2

Sutton R, Allen M (1997) Decadal predictability of north atlantic sea surface temperature and climate. Nature 388(6642):563–567

Svendsen L, Hetzinger S, Keenlyside N, Gao Y (2014) Marine-based multi-proxy reconstruction of atlantic multidecadal variability. Geophysical Research Letters 41(4):1295–1300, DOI 10.1002/2013GL059076

The Drakkar Group (2007) Eddy-permitting ocean circulation hindcasts of past decades. Clivar Exchanges (12):8–10

Timmermann R, Goosse H, Madec G, Fichefet T, Ethe C, Duliere V (2005) On the representation of high latitude processes in the orca-lim global coupled sea ice–ocean model. Ocean Modelling 8(1):175–201, DOI 10.1016/j.ocemod.2003.12.009

Visbeck M, Cullen H, Krahmann G, Naik N (1998) Ocean model's response to north atlantic oscillation-like wind forcing. Geophysical Research Letters 25(24):4521–4524

Visbeck M, Chassignet E, Curry R, Delworth T, Dickson R, Krahmann G (2003) The ocean's response to north atlantic oscillation variability. Geophysical Monograph-American Geophysical Union 134:113–146

Wang C, Zhang L (2013) Multidecadal ocean temperature and salinity variability in the Tropical North Atlantic: linking with the AMO, AMOC, and subtropical Cell. Journal of Climate 26(16):6137–6162, DOI 10.1175/JCLI-D-12-00721.1

Wunsch C (2005) The total meridional heat flux and its oceanic and atmospheric partition. Journal of climate 18(21):4374–4380, DOI 10.1175/JCLI3539.1

Zhai X, Johnson HL, Marshall DP (2014) A simple model of the response of the atlantic to the north atlantic oscillation. Journal of Climate (2014), DOI 10.1175/JCLI-D-13-00330.1

Zhang R (2008) Coherent surface-subsurface fingerprint of the atlantic meridional overturning circulation. Geophysical Research Letters 35(20), DOI 10.1029/2008GL035463

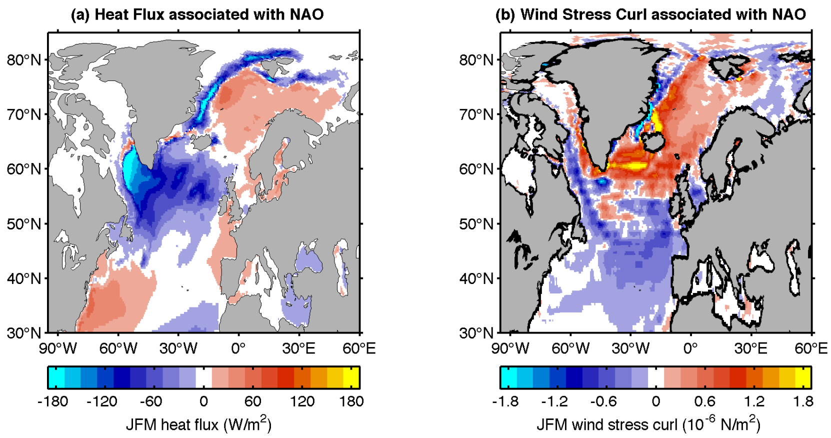

Fig. 1 (a) The mean winter (JFM) downward heat flux in years when the unfiltered NAO index is larger than plus one standard deviation, minus the mean over years when the unfiltered NAO index is more negative than minus one standard deviation. (b) Same as (a) but for the wind stress curl. A 9-point smoothing has been applied to the wind stress curl.

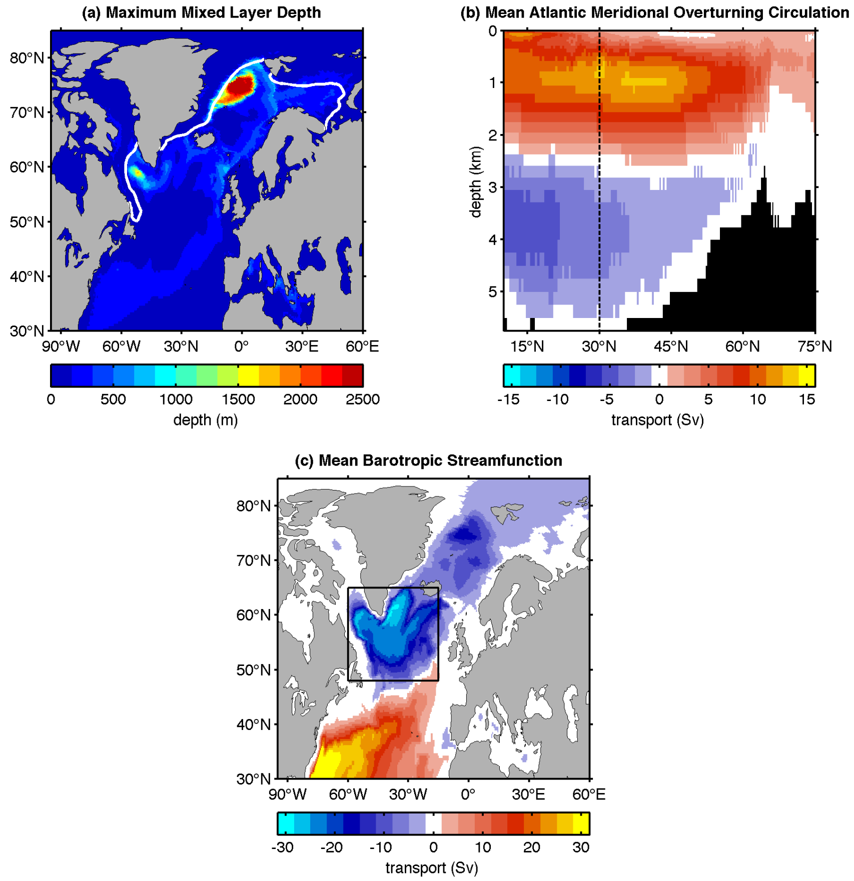

Fig. 2 (a) Mean of the maximum mixed layer depth in each year from the SF integration with white line indicating winter sea ice edge defined as the 0.5 contour of sea ice fraction (b) mean AMOC streamfunction from the SF integration with the dashed line indicating the 30°N latitude at which the AMOC index is calculated (c) mean barotropic streamfunction from the SF integration with the black box showing the area used to compute the SPG strength index.

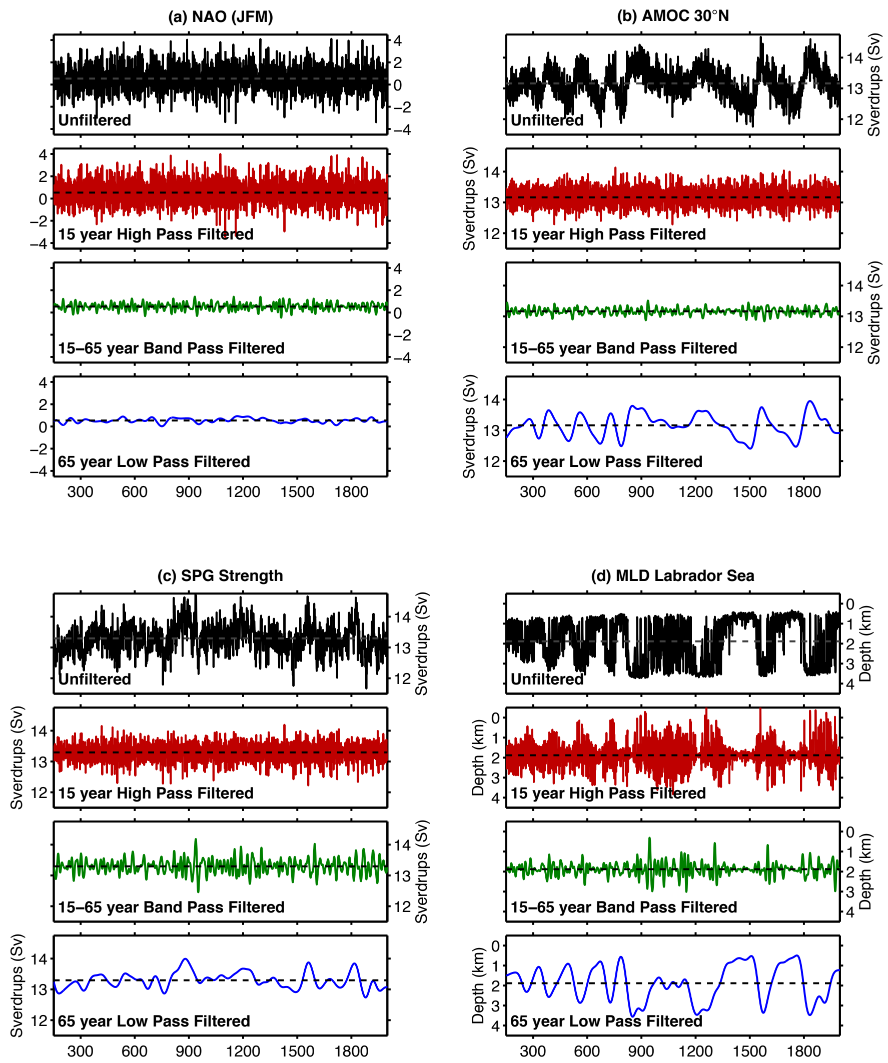

Fig. 3 Timeseries of (a) the winter (JFM) NAO, (b) AMOC at 30°N, (c) SPG Strength and (d) mixed layer depth in the Labrador Sea. The timeseries are unfiltered (black), filtered with a 15 year high pass filter (red), 15-65 year band pass filter (green) and 65 year low pass filtered (blue).

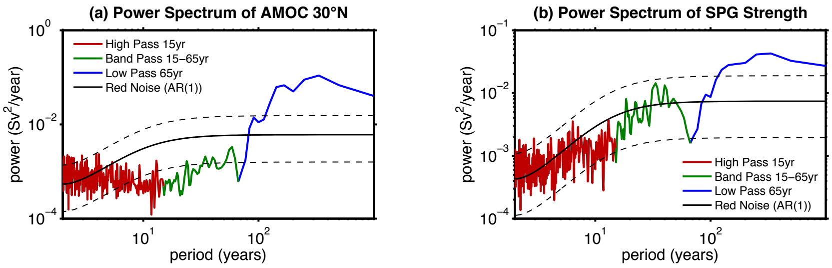

Fig. 4 The power spectrum of (a) the AMOC at 30°N and (b) the SPG Strength, divided into periods of 15 years or less (red), 15-65 years (green) and 65 years and longer (blue). The AR(1) fit is shown in black with dashed lines indicated the 95% confidence interval.

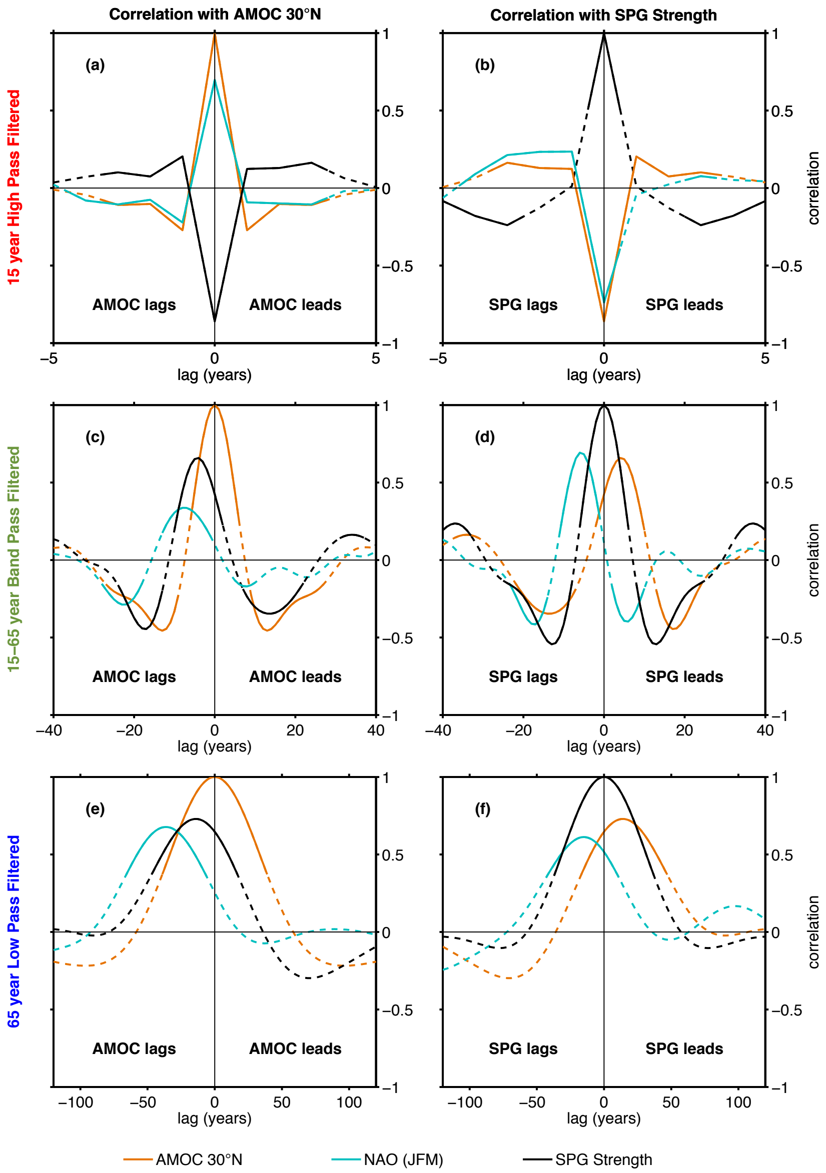

Fig. 5 (a) Auto-correlation of the 15 year high pass filtered AMOC at 30°N (light grey) and cross-correlations of the 15 year high pass filtered AMOC at 30°N with the 15 year high pass filtered NAO index (dark grey), and SPG strength (black). Correlations significant at 95% are shown with a solid curve while correlations not significant at the 95% level are shown with a dashed curve. Note that there appears to be significant correlations with value 0 because there is a sign switch between the significant correlations from one lag to the next. (b) Same as (a) but for the SPG strength. (c,d) same as (a,b) but for 15-65 year band pass filtered data. (e,f) same as (a,b) but for 65 year low pass filtered data.

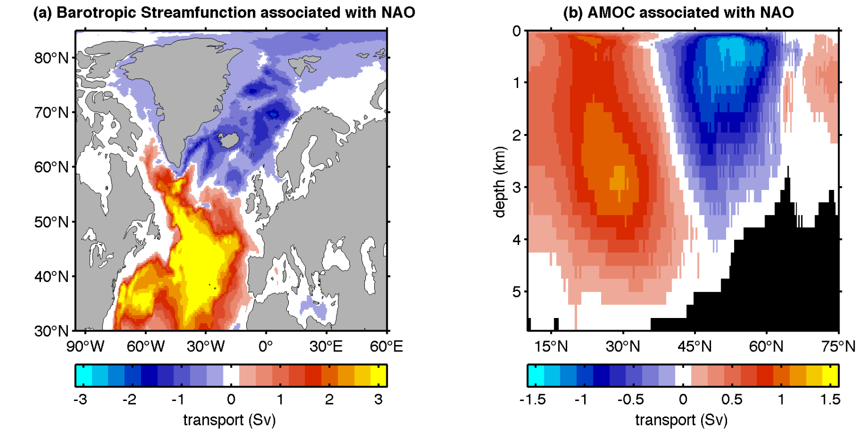

Fig. 6 (a) The mean barotropic streamfunction for years when the filtered NAO index is larger than plus one standard deviation, minus the mean for years when the filtered NAO index is more negative than minus one standard deviation from the mean. (b) same as (a) but for AMOC. The NAO index has been filtered with a 15 year high pass filter.

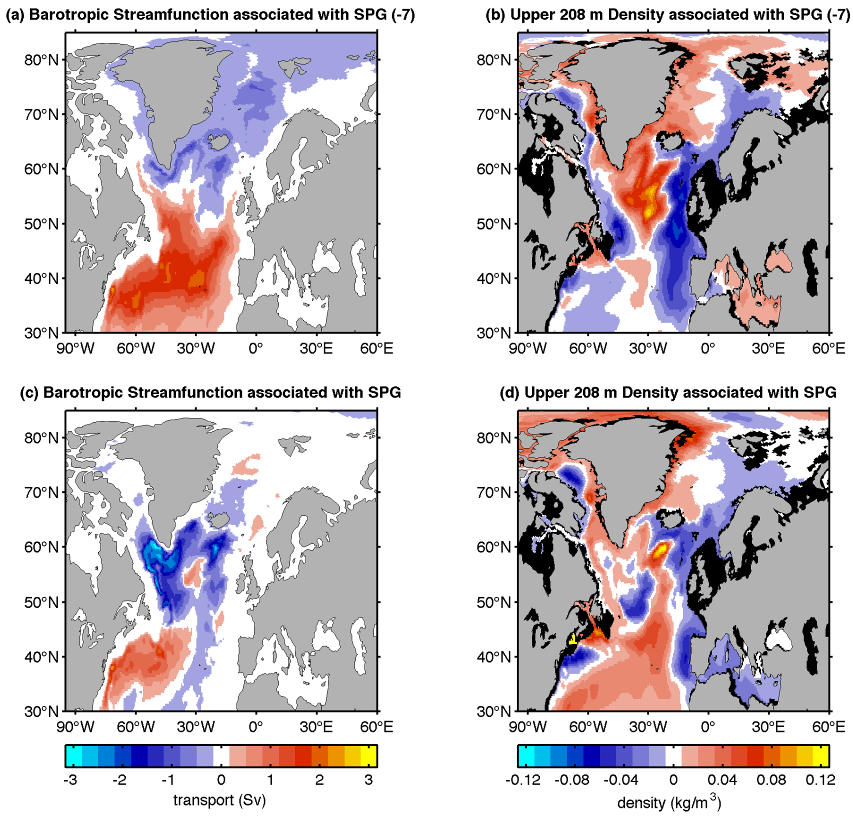

Fig. 7 (a) The mean barotropic sreamfunction 7 years before when the 15-65 year band pass filtered SPG strength is larger than plus one standard deviation, minus the mean over 7 years before when the 15-65 year band pass filtered SPG strength is more negative than minus one standard deviation. (b) Same as (a) but for the potential density in the upper 208 m. (c) same as (a) but in phase with the 15-65 year band pass filtered SPG strength. (d) same as (b) but in phase with the 15-65 year band pass filtered SPG strength.

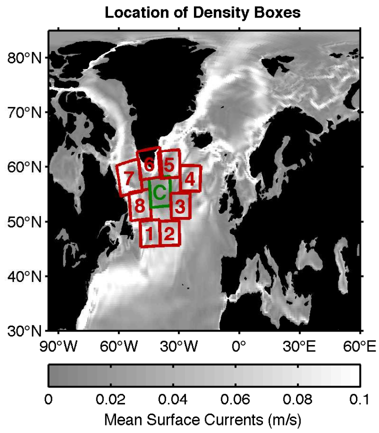

Fig. 8 Location of boxes at which density profiles have been computed. The shading shows the mean surface current speed from the SF integration.

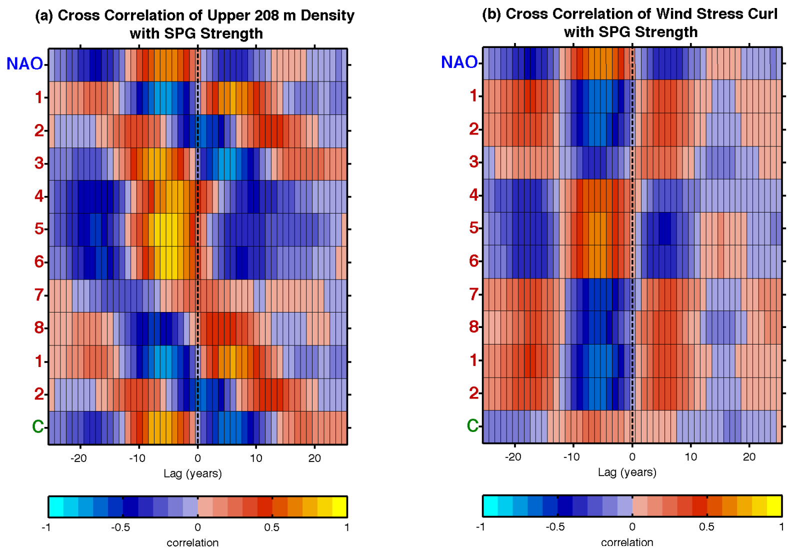

Fig. 9 (a) Cross-correlation between the 15-65 year band pass filtered SPG strength and the density of the upper 208 m in the boxes defined in Figure 8, as well as the NAO index. (b) Same as (a) but for mean wind stress curl in each box.

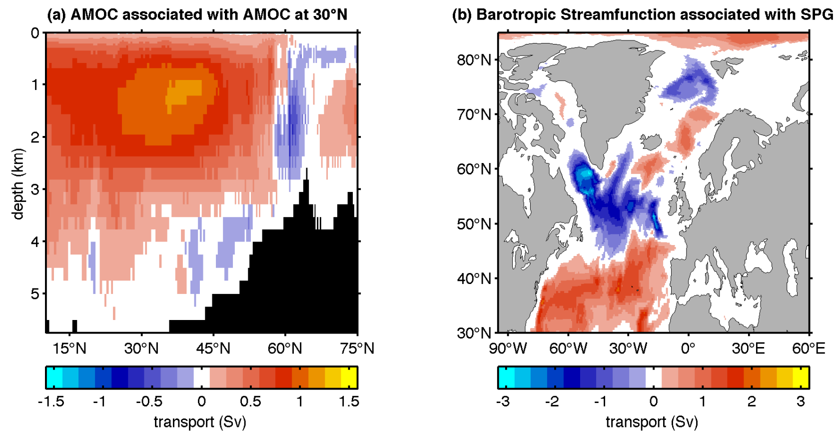

Fig. 10 (a) The mean AMOC over years when the 65 year low pass filtered AMOC index is larger than the mean AMOC index by more than one standard deviation, minus the mean over years when the filtered AMOC index is less than the mean minus one standard deviation. (b) Same as (a) but for the barotropic streamfunction with the SPG strength.

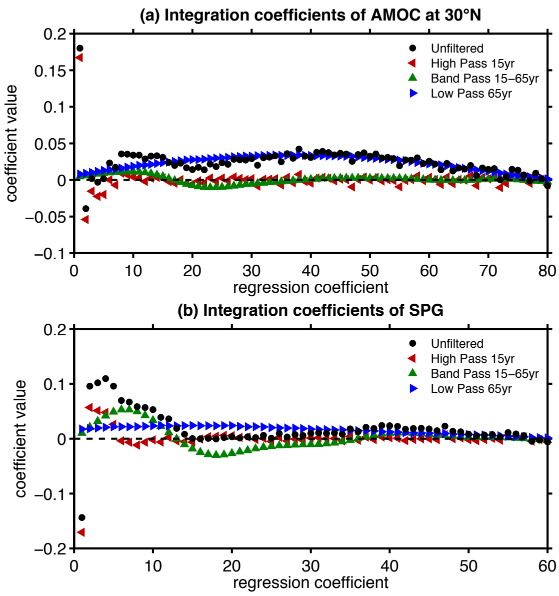

Fig. 11 Coefficients from the integrated NAO fit are shown for (a) the AMOC at 30°N for unfiltered data (black), 15 year high pass filtered data (red), 15-65 year band pass filtered data (green), and 65 year low pass filtered data (blue). (b) same as (a) but for the SPG Strength.